Nuclear Magnetic Resonance Acoustic Absorption in KI and KBr

D. I. Bolef and M. Menes
Westinghouse Research Laboratories, Pittsburgh, Pennsylvania
(Received January 28, 1959)

A technique for measuring the coupling between nuclear spins and the crystal lattice is described. The technique is one in which the absorption of energy by the nuclear spins from an acoustic wave is observed as an additional attenuation of the wave in the sample. This attenuation results in a change in the electric impedance of the piezoelectric transducer which drives the sample. The transducer impedance is made to control a Pound-Watkins type of spectrometer through an inverting and matching network.

Nuclear Magnetic Resonance acoustic absorption measurements were made on single crystal samples of KI and KBr using compressional waves in the [100] direction. These measurements yield a value of the electric quadrupole coupling e^2q_1Q, where q_1 is the first derivative with respect to strain of the electric field gradient at the nuclear position. For I^{127} in KI, $e^2q_1Q/h=300$ Mc/sec. For Br^{81} in KBr, $e^2q_1Q/h=82$ Mc/sec. Interpreting these results on the basis of a point charge model we obtain values of the amplification factor γ. For KI^{127}, $\gamma=38$. For KBr^{81}, $\gamma=26$.

INTRODUCTION

In many solids the dominant nuclear spin-lattice relaxation mechanism has been shown[1] to be due to the interaction between the nuclear electric quadrupole moment and the internal crystalline electric field gradient. The mechanism is one in which the thermal vibrations of the crystal lattice cause a time-dependent modulation of the electric field gradient. This modulation causes transitions among the nuclear spin energy levels. Because of the symmetry of the quadrupole interaction transitions involving $\Delta m=\pm 2$ as well as $\Delta m=\pm 1$ are allowed. The nuclear spins can interact with the lattice either by the direct (first-order) effect with the emission or absorption of a single phonon having frequency ν_0 or $2\nu_0$, or else by an indirect (Raman scattering type) process with the simultaneous emission and absorption of phonons differing in frequency by either ν_0 or $2\nu_0$. Except at extremely low temperatures the indirect process predominates in the spin-lattice relaxation.

The existence of a nuclear spin-lattice interaction has led to proposals[2,3] that the inverse process—the absorption by the nuclear spin system of energy from an externally generated acoustic wave—should be observable. This effect was first demonstrated in the acoustic saturation experiments of Proctor and Tantilla[4] in $NaClO_3$. Other workers extended this work to the study of alkali halides.[5–7] In these experiments acoustic energy of the proper frequency is introduced into the crystal sample. The absorption of energy from the sound wave causes the nuclear spin system to depart from a thermal distribution. This is observed as a decrease in the amplitude—a saturation—of the nuclear magnetic resonance signal.

The present paper describes a technique in which the absorption of energy by the nuclear spins is observed as an additional attenuation of the acoustic wave in the sample. As will be discussed below, the magnitude of this NMR acoustic attenuation depends primarily upon the strength of the coupling between the nuclear spins and the crystal lattice. Some preliminary results obtained by this technique have been reported.[8,9] This paper will discuss the application of NMR acoustic absorption techniques to single crystals of KI and KBr.

THEORY

The Quadrupole Interaction

NMR acoustic absorption differs from normal NMR primarily in the method of coupling to the nuclear spin system. In NMR, transitions are induced among the nuclear spin energy levels (shown in Fig. 1 for the high-field case with $I=\frac{5}{2}$) by the interaction of the rf magnetic field with the nuclear magnetic dipole moment. In NMR acoustic absorption, for the substances studied, transitions are induced among the same levels but by the interaction of the nuclear electric quadrupole moment with the electric field gradient produced by the lattice vibrations; thus, the selection rules and transition probabilities will differ from those in normal NMR.

The electric quadrupole interaction can be written

$$\mathcal{H}_Q=\mathbf{Q}:\nabla\mathbf{E}, \tag{1}$$

where $\mathbf{Q}$ is the nuclear electric quadrupole moment tensor, and $\nabla\mathbf{E}$ is the crystalline electric field gradient tensor. The effect of an acoustic wave is to create a time-varying strain in the locality of the nucleus. We are interested in that part of the electric field gradient which is a function of the strain. We therefore expand the electric field gradient components in a Taylor series of the strain components, obtaining to second order: (a) constant terms, (b) terms linear in the strain com-

[1] R. V. Pound, Phys. Rev. **79**, 685 (1950).
[2] A. Kastler, Experientia **8**, 1 (1952).
[3] S. A. Al'tshuler, J. Exptl. Theoret. Phys. U.S.S.R. **28**, 49 (1955) [translation: Soviet Phys. JETP **1**, 37 (1955)].
[4] W. G. Proctor and W. H. Tantilla, Phys. Rev. **101**, 1757 (1956).
[5] W. G. Proctor and W. Robinson, Phys. Rev. **104**, 1344 (1956).
[6] Jennings, Tantilla, and Kraus, Phys. Rev. **109**, 1059 (1958).
[7] E. F. Taylor and N. Bloembergen, Phys. Rev. **113**, 431 (1959).
[8] M. Menes and D. I. Bolef, Phys. Rev. **109**, 218 (1958).
[9] D. I. Bolef and M. Menes, Bull. Am. Phys. Soc. Ser. II, **3**, 144 (1958).

ponents, and (c) terms quadratic in the strain components. The constant terms are responsible for the zero-field quadrupole interaction which can be observed in many crystals. In the alkali halides these terms vanish because of cubic symmetry.

The linear terms are the ones which are of interest in this experiment. They relate the time-varying strain caused by the impressed sound wave to the time-varying electric field gradient. They similarly enter into the direct or single-phonon relaxation process. They also enter into the static broadening of the line shape by static strains due to imperfections in the crystal lattice.

The quadratic terms are the ones which enter into the indirect or Raman type of relaxation process. At room temperature the quadratic terms control the relaxation in those substances where the relaxation is through the quadrupole interaction.

At high magnetic fields, such that the quadrupole interaction is small compared to the separation of the magnetic energy levels, we have, in the notation of Pound,[1] the following nonzero matrix elements:

$$(m|\mathcal{H}_Q|m)=A[3m^2-I(I+1)](\nabla E)_0\cdots, \tag{2a}$$

$$(m|\mathcal{H}_Q|m\pm1)=\mp(6^{\frac{1}{2}}/2)A(2m\pm1)[(I\pm m+1)\times(I\mp m)]^{\frac{1}{2}}(\nabla E)_{\pm1}\cdots, \tag{2b}$$

$$(m|\mathcal{H}_Q|m\pm2)=(6^{\frac{1}{2}}/2)A[(I\mp m)(I\mp m-1)\times(I\pm m+1)(I\pm m+2)]^{\frac{1}{2}}(\nabla E)_{\pm2}\cdots, \tag{2c}$$

where $A=eQ/2I(2I-1)$, and Q is the electric quadrupole moment of the nucleus.

We restrict the discussion to the case of a longitudinal wave propagated in the direction of a cube axis. Under these conditions the field gradient resulting from the strain has axial symmetry along the direction of propagation. The field gradient elements can be written:

$$(\nabla E)_0=\tfrac{1}{4}eq(3\cos^2\theta-1), \tag{3a}$$

$$(\nabla E)_{\pm1}=\pm(1/4)(6^{\frac{1}{2}})eq\sin\theta\cos\theta e^{\pm i\varphi}, \tag{3b}$$

$$(\nabla E)_{\pm2}=(1/8)(6^{\frac{1}{2}})eq\sin^2\theta e^{\pm i\varphi}, \tag{3c}$$

where θ is the angle between the axis of symmetry and the direction of the main magnetic field, and φ is the angle between the projection of the symmetry axis on the xy plane and the x-axis. The scalar quantity q is a measure of the magnitude of the axially symmetric field gradient. The Taylor expansion of the field gradient in terms of the strain then becomes, similar to the case of diatomic molecules,[10]

$$q=q_0+q_1[(r-a)/a]+\tfrac{1}{2}q_2[(r-a)/a]^2+\cdots, \tag{4}$$

where $(r-a)/a=\delta$ is the strain caused by the longitudinal sound wave; q_1 and q_2 are the Taylor expansion coefficients and are therefore, respectively, the first and second derivatives of q with respect to δ.

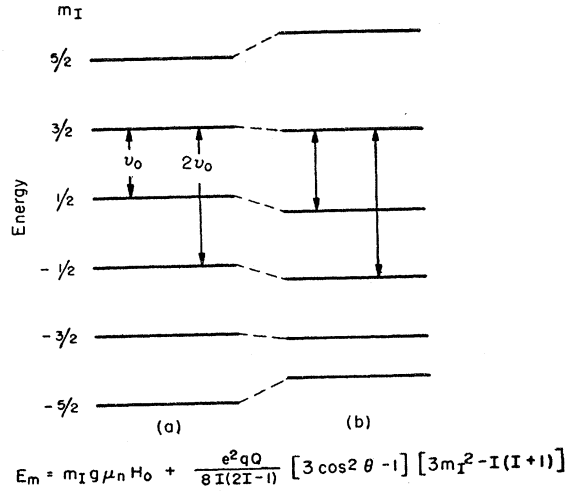

FIG. 1. High-field energy levels for spin $I=\frac{5}{2}$. (a) No static quadrupole interaction. ν_0 and $2\nu_0$ correspond to single-frequency ($\Delta m=\pm1$) and double-frequency ($\Delta m=\pm2$) transitions. (b) Effect of static quadrupole interaction.

TABLE I. High-field transition frequencies and transition probabilities in NMR and NMR acoustic absorption for nucleus with spin $I=\frac{5}{2}$.

	NMR ($\Delta m=\pm1$)		Acoustic ($\Delta m=\pm1$)			Acoustic ($\Delta m=\pm2$)	
Trans.	Trans. freq.	Trans. prob.	Trans. freq.	Trans. prob.	Trans.	Trans. freq.	Trans. prob.
$\frac{3}{2}\leftrightarrow\frac{5}{2}$	$\nu_0+12\Delta$	5	$\nu_0+12\Delta$	5	$\frac{1}{2}\leftrightarrow\frac{5}{2}$	$2\nu_0+18\Delta$	5
$\frac{1}{2}\leftrightarrow\frac{3}{2}$	$\nu_0+6\Delta$	8	$\nu_0+6\Delta$	2	$-\frac{1}{2}\leftrightarrow\frac{3}{2}$	$2\nu_0+6\Delta$	9
$-\frac{1}{2}\leftrightarrow\frac{1}{2}$	ν_0	9					
$-\frac{3}{2}\leftrightarrow-\frac{1}{2}$	$\nu_0-6\Delta$	8	$\nu_0-6\Delta$	2	$-\frac{3}{2}\leftrightarrow\frac{1}{2}$	$2\nu_0-6\Delta$	9
$-\frac{5}{2}\leftrightarrow-\frac{3}{2}$	$\nu_0-12\Delta$	5	$\nu_0-12\Delta$	5	$-\frac{5}{2}\leftrightarrow-\frac{1}{2}$	$2\nu_0-18\Delta$	5

$(\nabla E)_0$ enters into the static splitting of the high-field energy levels. To first order, the levels are shifted by an amount $[e^2qQ/8I(2I-1)][3m^2-I(I+1)](3\cos^2\theta-1)$ as shown in Fig. 1. $(\nabla E)_{\pm1}$ and $(\nabla E)_{\pm2}$ enter into the transition probabilities for $(\Delta m=\pm1)$ and $(\Delta m=\pm2)$, respectively. We term these the single-frequency and double-frequency transitions. From perturbation theory the transition probability is given by $W_m=(1/4\hbar^2)\times\langle m|H_1|m'\rangle^2 g(\nu)$, where $g(\nu)$ is the shape function of the absorption line. Using the matrix elements for axial symmetry [Eqs. (2b) and (2c), and (3b) and (3c)] one obtains for the transition probabilities due to a time-varying electric field gradient having peak value q:

$$W_{Q1}=W_{m,\,m\pm1}=(9\pi^2/16h^2)e^2A^2q^2(2m+1)^2\times(I\pm m+1)(I\mp m)\sin^2\theta\cos^2\theta\, g(\nu), \tag{5a}$$

$$W_{Q2}=W_{m,\,m\pm2}=(9\pi^2/64h^2)e^2A^2q^2\times(I\mp m)(I\mp m-1)(I\pm m+1)\times(I\pm m+2)\sin^4\theta\, g(\nu), \tag{5b}$$

$$W_M=W_{m,\,m\pm1}=(1/4)\gamma^2H_1^2(I\mp m)\times(I\pm m\mp1)\sin^2\theta\, g(\nu). \tag{5c}$$

[10] H. J. Zeiger and D. I. Bolef, Phys. Rev. **85**, 788 (1952).

For comparison the transition probability for normal NMR is given in (5c). There γ is the nuclear magnetogyric ratio, $2H_1$ is the peak value of the rf magnetic field, and θ the latter's angle with the static field H_0.

The transition frequencies and transition probabilities for the case of a quadrupole split high-field line are given in Table I for a nuclear spin of $\frac{5}{2}$, and in Table II for a nuclear spin of $\frac{3}{2}$. The quantity ν_0, the unperturbed level separation, is given by $\nu_0=\mu g H_0/h$. The quadrupole splitting is given in units of a quantity $\Delta=(e^2qQ/80h)\times(3\cos^2\theta-1)$ for $I=\frac{5}{2}$, and $\Delta=(e^2qQ/24h)(3\cos^2\theta-1)$ for $I=\frac{3}{2}$. The transition probabilities are given in relative terms. Of particular interest is the absence of the central component ($-\frac{1}{2}$ to $+\frac{1}{2}$) for the acoustic lines, and the relative weighting between the inner and the outer satellite transitions for the NMR and the single-frequency and double-frequency acoustic lines.

NMR Acoustic Absorption Coefficient

Let the coefficient of the acoustic absorption due to the nuclear spin system be α_n. The power absorption

TABLE II. High-field transition frequencies and transition probabilities in NMR and NMR acoustic absorption for nucleus with spin $I=\frac{3}{2}$.

	NMR ($\Delta m=\pm1$)		Acoustic ($\Delta m=\pm1$)			Acoustic ($\Delta m=\pm2$)	
Trans.	Trans. freq.	Trans. prob.	Trans. freq.	Trans. prob.	Trans.	Trans. freq.	Trans. prob.
$+\frac{1}{2}\leftrightarrow+\frac{3}{2}$	$\nu_0+2\Delta$	3	$\nu_0+2\Delta$	3	$-\frac{1}{2}\leftrightarrow\frac{3}{2}$	$2\nu_0+2\Delta$	3
$-\frac{1}{2}\leftrightarrow+\frac{1}{2}$	ν_0	4					
$-\frac{3}{2}\leftrightarrow-\frac{1}{2}$	$\nu_0-2\Delta$	3	$\nu_0-2\Delta$	3	$-\frac{3}{2}\leftrightarrow\frac{1}{2}$	$2\nu_0-2\Delta$	3

coefficient, $2\alpha_n$, is then given by $2\alpha_n=P_n/P_0$, where P_n is the power per unit volume absorbed by the nuclei and P_0 the power per unit area in the acoustic wave. The power absorbed by the nuclei is

$$P_n=[N/(2I+1)][(h\nu)^2/kT]\sum W_Q,$$

where N is the number of spins per cm^3, T is the absolute temperature and the summation is taken over those transitions contributing to the line. The power density in the acoustic wave is given by

$$P_0=\tfrac{1}{2}\rho c^3\delta^2.$$

Here ρ is the density of the material, c is the velocity of the wave, and δ is the peak value of the time-varying strain caused by the sound wave.

Using the transition probabilities given by (5a) and (5b), and using the linear term in the Taylor expansion for q [Eq. (4)], together with the above, one obtains for $I=\frac{5}{2}$

$$\alpha_{m,\,m+2}=(21\pi^2/1600)(Ne^4Q^2/\rho c^3kT)\nu^2g(\nu)q_1^2\sin^4\theta, \quad (6a)$$

$$\alpha_{m,\,m+1}=(21\pi^2/400)(Ne^4Q^2/\rho c^3kT)\times\nu^2g(\nu)q_1^2\sin^2\theta\cos^2\theta, \quad (6b)$$

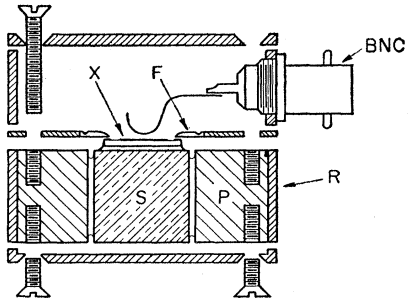

FIG. 2. NMR acoustic absorption probe. S is the single crystal sample, X the quartz transducer bonded to the sample, F a spring washer to provide ground contact, P a plastic block in which the sample is held, and R an aluminum ring with top and bottom caps to provide shielding.

and for $I=\frac{3}{2}$

$$\alpha_{m,\,m+2}=(3\pi^2/128)(Ne^4Q^2/\rho c^3kT)\nu^2g(\nu)q_1^2\sin^4\theta, \quad (6c)$$

$$\alpha_{m,\,m+1}=(3\pi^2/32)(Ne^4Q^2/\rho c^3kT)\times\nu^2g(\nu)q_1^2\sin^2\theta\cos^2. \quad (6d)$$

EXPERIMENTAL APPARATUS AND PROCEDURE

The experimental problem is to detect and measure a small increase in the acoustic attenuation of the sample material, of the order of 10^{-8} cm^{-1}. In essence the method is the following. The sample material is prepared to be mechanically resonant. A quartz transducer crystal is bonded to the sample. Under conditions of mechanical resonance of the sample the acoustic impedance seen by the transducer, and therefore the electrical impedance presented by the transducer, is a function of the acoustic attenuation of the sample material. By means of an appropriate matching network, the electrical impedance of the transducer is made to control a Pound-Watkins spectrometer. The latter thus becomes sensitive to small changes in acoustic attenuation of the sample.

Sample Preparation and Mounting

The samples used were single crystals of KI and KBr obtained from Harshaw Chemical Company. The samples were generally cubical in shape and large enough to accommodate a $\frac{1}{2}$-inch diameter transducer. The two faces normal to the sound direction were finished flat and parallel to less than 0.0001 inch over the area covered by the transducer. The samples were ground in a jig on successively finer grades of polishing paper, followed by American Optical 303$\frac{1}{2}$ powder and a final polish on cloth with Linde type A sapphire. Kerosene was used in these operations.

The sample is mounted as shown in Fig. 2. The sample is cemented in a plastic block. An aluminum ring fits around this plastic block and together with the top and bottom caps makes up the shielded sample enclosure.

The transducers were quartz, fundamental, X-cut, and of $\frac{1}{2}$-inch diameter. They were cemented to the sample by a room-temperature-setting epoxy resin (Bakelite C-8). Care was taken to make as thin a joint as possible and to exclude dust and small bubbles from the bond. The resin was allowed to set with moderate pressure at a slightly elevated temperature (45°C) for twelve hours. Electrical contact to the top crystal plating was made by a gold wire whisker. The bottom plating was "wrap around"; it extended around the sides to a narrow ring on the top surface of the transducer crystal. Contact was made with this ring by a circular set of fingers.

Acoustic Properties of the Sample and its Equivalent Circuit

The sample is mechanically resonant at a discrete set of frequencies corresponding to standing wave patterns containing integral numbers of half wavelengths. The effect of these sample resonances on the electrical characteristics of the transducer can be obtained most simply from consideration of the equivalent circuit shown in Fig. 3(a).[11]

Under the assumption that the wave propagation is one-dimensional, the sample can be represented by a short-circuited transmission line having surge impedance Z, length l, attenuation α. Z is a function of the acoustic characteristics of the sample: $Z=\rho cS$, where ρ is the sample density, c the velocity of sound, and S is the cross sectional area of the wave pattern. The bond is equivalent to a short length of transmission line and is represented by a tee section. The transducer is represented by its conventional equivalent circuit, which is valid for frequencies near the transducer resonance and for load impedances small compared to the transducer characteristic impedance. Both of these conditions are well satisfied. The electromechanical transformation properties of the transducer are represented by the ideal transformer of ratio $1:2a$. It transforms the mechanical quantities on the right into electrical quantities as seen from the left. For an X-cut air-backed transducer the electromechanical transformation factor is $2a=2e_{11}A/t$, where e_{11} is the appropriate piezoelectric stress constant (0.18 mks units), A is the active transducer area and t is the transducer thickness.

The acoustic impedance presented by the sample may be derived from transmission line theory. It is found that in the vicinity of a mechanical resonance, and for the condition $\alpha l \ll 1$, the sample impedance behaves like a series RLC circuit. This is shown in Fig. 3(b), where the electromechanical transformation has also been performed and all quantities are in electrical units. The value of R, the resonant transducer resistance, is given by:

$$R=(1/2a)^2\rho cSl\alpha. \tag{7}$$

It was found that for the samples used the bond could be neglected. The equivalent circuit then reduces to that shown in Fig. 3(c).

In actuality the problem is not purely one dimensional; there is some beam spreading. The effect of this beam spreading is two-fold: It causes the standing wave pattern to cover an area larger than the transducer; and it also causes shear wave conversion where the beam meets the sample sides so that the standing wave pattern is not purely longitudinal. The first effect is allowed for by obtaining the effective area of the standing wave pattern from independent measurements of both the transducer resistance and the attenuation coefficient. The shear mode conversion problem is more difficult. An approach to this problem based on numerical solution of the Pochhammer equations has been made by McSkimin[12] and by Taylor.[7] Their results can be expected to apply only qualitatively since the Pochhammer equations refer to a long cylindrical rod, while the present sample is nearly cubical. Their results indicate, however, that only a small fraction of the energy (of the order of 1 percent) is present in shear mode. No attempt is made in this paper to correct for shear mode conversion.

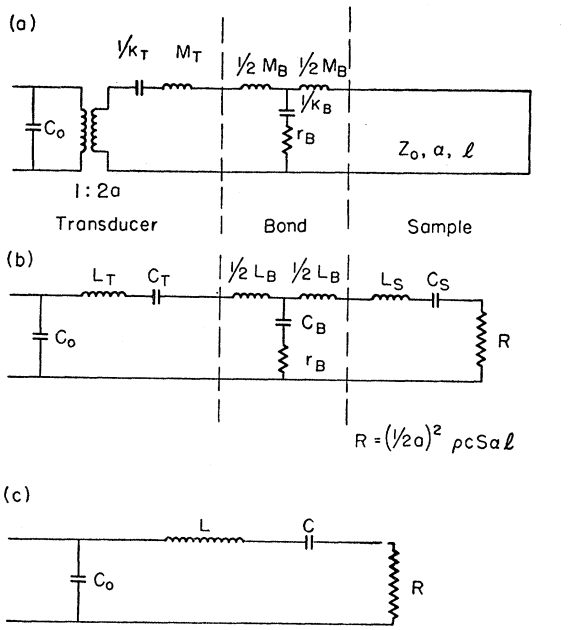

FIG. 3. Equivalent circuit of transducer-sample assembly. (a) From left to right: equivalent circuits of the transducer, bond, and sample. The latter is represented by a short-circuited transmission line. (b) Equivalent circuit after electromechanical transformation has been made and a series RLC equivalent circuit substituted for the transmission line. This is valid in the vicinity of a mechanical resonance. (c) Final equivalent circuit after bond is neglected.

[11] For a discussion of equivalent circuits, the transmission line analogy, the concept of acoustic impedance, etc., see, for instance, T. F. Hueter and R. H. Bolt, *Sonics* (John Wiley & Sons, Inc., New York, 1955).

[12] H. J. McSkimin, J. Acoust. Soc. Am. **28**, 484 (1956).

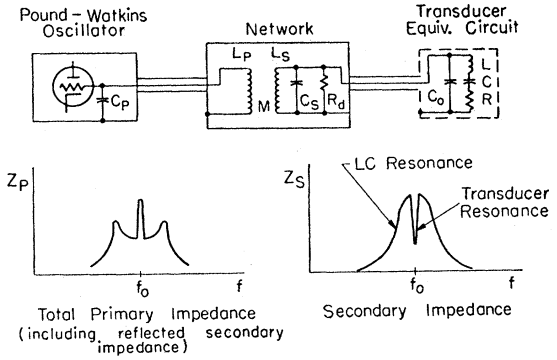

FIG. 4. Matching and inverting network. The impedance inversion at transducer resonance is shown in the bottom half of the figure.

Matching Network and NMR Equipment

The NMR acoustic absorption manifests itself by a small increase in the sound attenuation of the sample. This is reflected as a small change in the resistive component of the transducer. It is the function of the NMR equipment to detect this small change. This is achieved by allowing the transducer to control a Pound-Watkins oscillator. Because the transducer exhibits an impedance minimum at sample resonance, while a two-terminal oscillator like the Pound-Watkins oscillates at an impedance maximum, an inverting network is interposed between the transducer and the oscillator. This network also serves the purpose of selecting the desired sample resonance and of matching the transducer impedance to a value acceptable to the oscillator.

We have used a pair of overcoupled tuned circuits for the inverting network. The network is shown schematically in Fig. 4, with an indication of how the transducer impedance dip is inverted into an impedance peak. The additional damping resistor, R_d, is necessary to bring the side peaks of the overcoupled circuit response down below the sample resonance peak; this forces the oscillator to oscillate at the desired sample resonance frequency. (See Appendix.)

The remainder of the equipment is fairly conventional. The Pound-Watkins oscillator, in addition to the long time constant feedback, also has some audio frequency feedback.[13] This feature allows stable operation over a wider range of conditions. The calibrator is similar to the one described by Watkins,[14] but uses, instead of the plate resistance of a vacuum tube, a bolometer fuse as the modulated conductance. The calibrator was made absolute by bridge measurement of the bolometer characteristic. For absolute quantitative NMR measurements, it is also necessary to know the filling factor of the coil. This filling factor was measured by inserting a small copper sphere at various positions in the coil and noting the frequency shift of the oscillator.[15]

The magnetic field was provided by a Varian 12-inch magnet with 2.5-in. pole gap. Magnetic field modulation at 24 cps and synchronous detection were used. The field sweep was of the order of 1 gauss per minute. In the NMR work, resonances were observed with two values of ac field modulation: a low amplitude modulation was used to observe the center of the line; and a high amplitude modulation was used to observe the wings of the line. Typical values of ac modulation were 0.2 gauss and 1.6 gauss peak to peak. Since the NMR acoustic absorption lines do not show a sharp central component, only the large value of field modulation was used in observing them. All measurements were made at room temperature.

EXPERIMENTAL RESULTS

Acoustic Properties

Observations of the NMR acoustic absorption signal were made on a crystal of KI and on a crystal of KBr. The best results were obtained for the KI crystal (identified as KI No. 1) and the discussion will be primarily for that sample.

The KI No. 1 sample had a length of 1.48 cm, and a cross section of 1.42 cm by 1.29 cm. All faces were cleavage planes except for the end faces which were ground and polished. The transducer was an 8 Mc/sec fundamental X-cut quartz plate. Its nominal diameter was $\frac{1}{2}$ inch but because of the wrap-around plating its active area was 0.86 cm^2.

Figure 5 shows the comb pattern of the mechanical resonances for KI No. 1. The transducer conductance $(1/R)$ for each resonance is plotted against the frequency of the resonance. The widths of the resonances are of the order of one hundred cps, and are too narrow to show. Most of the data were taken at the 7.908

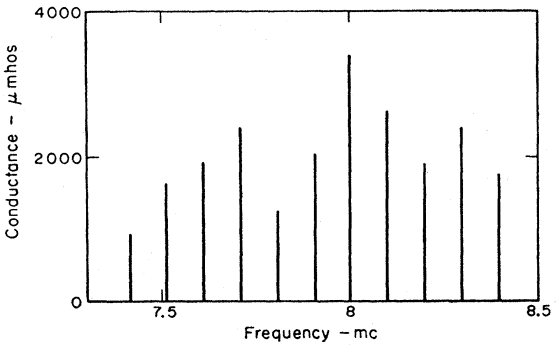

FIG. 5. Comb pattern of sample mechanical resonances for KI No. 1. Transducer conductance $(1/R)$ at peak of resonance is plotted against frequency of resonance. Widths of resonances are of the order of 100 cps.

[13] The use of af negative feedback in stabilizing an oscillator has been mentioned by R. J. Blume in Rev. Sci. Instr. **29**, 574 (1958).

[14] G. D. Watkins, Ph.D. dissertation, Harvard, 1952 (unpublished).

[15] The use of this method for measuring fields in microwave cavities is described by L. C. Maier, Jr., and J. C. Slater in J. Appl. Phys. **23**, 68 (1952).

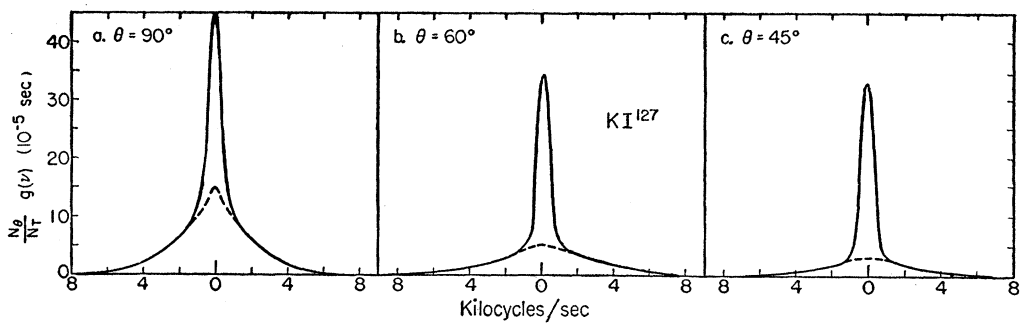

FIG. 6. NMR absorption line of I^{127} in KI at three values of the angle θ between the [100] axis and the magnetic field. af modulation of the central portion of the line was 0.2 gauss, of the wings 1.6 gauss. The absorption line is plotted as a shape function $(N_\theta/N_t)g(\nu)$, which integrates to unity over the expected line. The dotted line represents that part of the absorption line attributed to the satellite transitions.

Mc/sec resonance. The measured transducer conductance at that frequency was 2040 micromhos.

The influence of the resin bond on the acoustic characteristics of the sample assembly is primarily due to its shunt compliance. In terms of the equivalent circuit of Fig. 3(b) this compliance is represented by a capacitance C_B and a resistance r_B. To obtain these quantities measurements were made of the transducer bandwidth both under CW resonance conditions and under pulse conditions. The CW resonance bandwidth is represented by the envelope of the comb pattern of Fig. 5. It can be interpreted in terms of the equivalent circuit of Fig. 3(b). The pulse bandwidth was obtained from echo amplitudes as measured on a pulse-echo apparatus. This bandwidth can be interpreted in terms of the equivalent circuit of Fig. 3(b) with, however, the sample represented not by an *RLC* circuit, but by a simple resistance equal to its surge impedance. This is because for pulses shorter than a round trip time the sample appears infinite. The results of such bandwidth measurements for KI No. 1 give $1/2\pi fC_B = 300\,000$ ohms, and $r_B = 30\,000$ ohms. These electrical quantities correspond to a bond thickness of 0.28×10^{-3} inch and a mechanical Q for the resin of about 10. The magnitude of the shunt impedance is seen to be very much greater than the resonant sample impedance, and its neglect in going from Fig. 3(b) to Fig. 3(c) is thus justified.

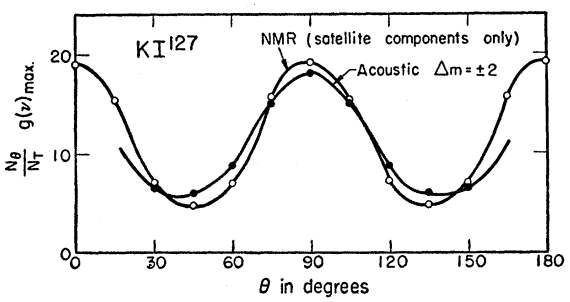

FIG. 7. Variation with θ of observed peak intensity of (a) the satellite part of the NMR line in KI^{127} and (b) the observed acoustic double-frequency ($\Delta m = \pm 2$) line in KI^{127} No. 1. The vertical scale is in units of 10^{-5} second. $(N_\theta/N_t)g(\nu)_{\max}$ is the peak value of the absorption line shape function plotted in Fig. 6. Its reciprocal quantity is the line width. The acoustic variation is obtained from Fig. 12 by dividing the observed peak absorption by the transition probability.

A measurement of the time constant of the 7.908 Mc/sec resonance of KI No. 1 was made by a free ringing method. The observed value was 2.2 milliseconds. The attenuation coefficient computed from this value is 0.00155 cm^{-1}. From this attenuation coefficient and from the measured transducer resistance the effective area (S) of the standing wave can be determined to be 1.66 cm^2. This area can be compared with an active transducer area of 0.86 cm^2 and a total sample area of 1.83 cm^2.

A summary of the acoustic properties of both samples is given in Table III.

NMR Results

An understanding of the normal NMR lines was found to be essential to the interpretation of the acoustic resonance results. Of interest were (a) the variation of signal amplitude and of line shape with crystal orientation and (b) the total integrated intensity of the NMR line. The former was useful in understanding the angular variation of the acoustic absorption line intensity. The latter was necessary for the determination of the magnitude of the nuclear electric quadrupole interaction from the observed integrated intensity of the acoustic line.

Previous investigators[14] have reported that the observed intensity of NMR lines in KI and KBr is less than the expected intensity computed from the number of spins present in the sample. This has been generally ascribed to the broadening and resulting loss (partial or complete) of that part of the line due to satellite transitions. The broadening is caused by a distribution

TABLE III. Acoustic properties.

	$(1/2a)$ (mks unit)	ρ (g/cc)	c (10^5 cm/sec)	l (cm)	S (cm^2)	R (ohm)
KI No. 1	12.1	3.13	2.90	1.48	1.66	490
KBr No. 1	10.5	2.75	3.56	1.49	2.0	925

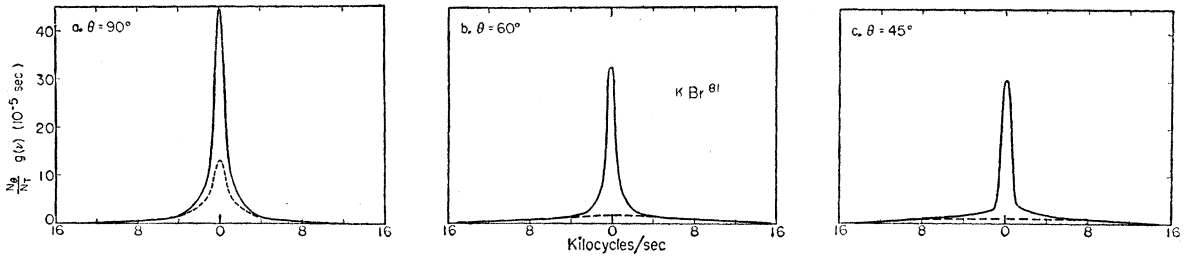

FIG. 8. NMR absorption lines of Br^{81} in KBr No. 1 at three values of θ. af modulation as in Fig. 6. The dotted lines represent that part of the absorption attributed to the satellite transitions.

of electric field gradients due to imperfections and residual strains in the crystal lattice. Since the acoustic absorption line consists of satellite transitions only, it is important to know what fraction of expected transitions is represented by the observed signal. This fraction has been obtained by comparison with the NMR signal. Such a procedure is, of course, not quite correct. The ratio of observed intensity to expected intensity is not a physical property of the sample; it is rather a function of the response of the instrumental system to a certain line shape. (The line shape is a property of the sample.) However, for line shapes which are similar such a comparison should be fairly reliable.

NMR runs were therefore made at several orientations of the crystal relative to the direction of the magnetic field. The NMR sample of KI was cleaved from the same crystal as the acoustic sample and was contiguous with it. The sample was positioned in the field so that the [100] axis along which the sound was to be propagated could be oriented in a plane containing the field direction. This makes the angle θ between these directions the same as θ of Eq. (3).

The rf level during the NMR runs was generally maintained at 11 milligauss rms for KI and 8 milligauss rms for KBr. Saturation began to be noticeable at levels of 19 milligauss for KI and 13 milligauss for KBr.

The NMR absorption line of I^{127} in KI is given in Fig. 6 for values of the angle θ of 90°, 60°, and 45°. The magnetic field was 9.3 kilogauss. The first order broadened satellite components are evident for the 60° and 45° lines. No second order effect on the central component could be detected in these runs. A comparison of the line shapes for various values of θ shows that the broadening of the satellite component is a function of the angle θ.

The intensity of the I^{127} NMR line in KI was measured by two methods. The first involved a comparison of the integrated intensity of the line with that due to a known number of Na^{23} spins in a single crystal of NaI. The second involved the absolute calibration of the calibrator and a measurement of the coil filling factor as described above. The first method gave a ratio of measured intensity to expected intensity of 85% for the 90° line while the second method gave a ratio of 79%. In calculations we used a mean value of 82%.

For the purpose of comparison with the acoustic absorption line we are interested in that part of the NMR line which corresponds to the satellite transitions and which is therefore affected in a similar manner by the stray electric field gradients. We assume that the $(-\frac{1}{2}$ to $+\frac{1}{2})$ transition contributes 100% of its possible intensity at all angles θ. Using the lines shown in Figs. 6(b) and 6(c), in which the spread-out wings are well resolved from the sharp central component, we may estimate the shape of this central component such that its area corresponds to 100% expected intensity. Subtracting this central component from the total lines gives the areas below the dotted lines. These dotted lines then denote the NMR line due to the satellite $(\pm\frac{1}{2}$ to $\pm\frac{3}{2})$ and $(\pm\frac{3}{2}$ to $\pm\frac{5}{2})$ transitions only. The ratio of observed intensity to expected intensity was found above to be 82% for the 90° KI line. Using this value, and assuming that the central component is all there (100%), we obtain a value of 74% for the ratio of observed to expected intensity of the satellite part of the line for $\theta=90°$.

We introduce a ratio of observed number of spins to total spins, N/N_t, as equal to the ratio of observed integrated line intensity to expected integrated line intensity. To describe the line we use a function $g(\nu)$ such that its integral over the observed line shape is unity. The true line shape function is then $(N/N_t)g(\nu)$, which would integrate to unity over the expected line. Results are shown in terms of this latter quantity; since it is a function of the angle θ we term it $(N_\theta/N_t)g(\nu)$.

The peak value of $(N_\theta/N_t)g(\nu)$ for the satellite part of the NMR line is shown in Fig. 7 as a function of θ. The vertical scale is in units of 10^{-5} sec. Also shown is the corresponding curve for the double-frequency acoustic transition. The angular variation of $(N/N_t)g(\nu)$ indicates that the strains which are responsible for the stray electric field gradients are not random, but possess preferred orientations.[16,17]

The NMR absorption lines of Br^{81} in the KBr No. 1 sample are shown in Fig. 8. The magnetic field was

[16] An analysis of the effect of dislocation introduced by plastic deformation on the NMR line shape in KI^{127} has been made by E. Otsuka, J. Phys. Soc. Japan **13**, 1155 (1958).

[17] The density of dislocations in KI has been estimated by J. H. Parker (of these Laboratories) from etch pits to be of the order of 10^6 per cm^2.

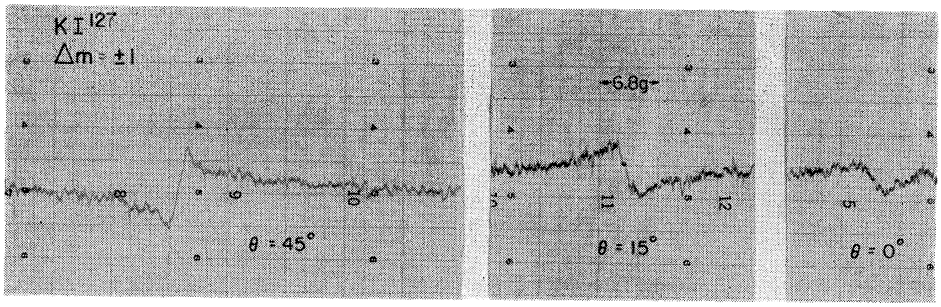

FIG. 9. Recorder traces of NMR acoustic absorption single-frequency lines of I^{127} in KI No. 1. The traces are derivatives of the actual absorption lines. θ is the angle between the acoustic axis and the direction of the external field. $H_0=9.22$ kgauss. $f=7.90$ Mc/sec. af modulation was 2 gauss peak to peak.

8.4 kilogauss. The behavior of the line shape and peak intensity for various angles θ is similar to that of I^{127} in KI. An intensity measurement, as described above, gave a value of 86% for the ratio N/N_t for the 90° line. Using the analysis described above for KI, we obtain a value of 77% for the ratio of observed to expected intensity of the satellite part of the KBr^{81} line.

NMR Acoustic Absorption Results

The NMR acoustic absorption lines were observed using the acoustic probe, matching network, and NMR spectrometer components described above. The magnetic field was adjusted to the resonant value H_0 for the single-frequency ($\Delta m=\pm 1$) acoustic absorption line. To observe the double-frequency ($\Delta m=\pm 2$) line the magnetic field was reduced to $H_0/2$. The KI absorption lines were observed at an rf amplitude at the Pound-Watkins oscillator of 0.5 volt rms, corresponding to a power input to the transducer of 8×10^{-5} watt. Saturation of the acoustic absorption line began to be noticeable at a level of 0.7 volt rms at the oscillator. The intensity of the acoustic absorption line was measured by the bolometer calibrator.

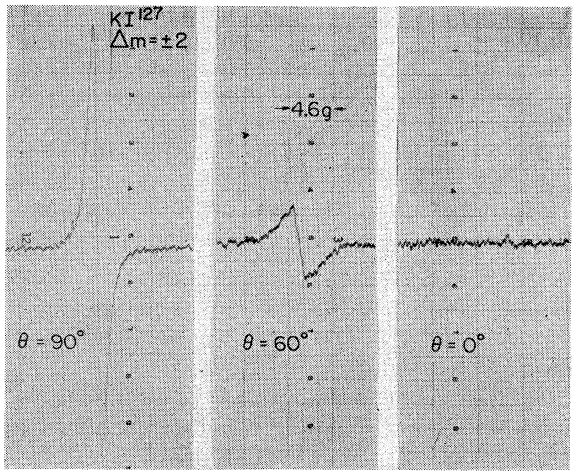

FIG. 10. Recorder traces of NMR acoustic absorption double-frequency lines of I^{127} in KI No. 1. The traces are derivatives of the actual absorption lines. θ is the angle between the acoustic axis and the direction of the external field. $H_0=4.6$ kgauss, $f=7.90$ Mc/sec. af modulation was 2 gauss peak to peak.

The observed lines of I^{127} in KI No. 1 are shown in Figs. 9 and 10 for several values of the angle θ between the axis of acoustic propagation and the direction of the magnetic field. In Fig. 9 are shown the acoustic single-frequency lines at a frequency $f_0=7.90$ Mc/sec and magnetic field $H_0=9.22$ kilogauss. In Fig. 10 are shown the acoustic double-frequency lines at the same frequency but at a magnetic field equal to 4.61 kilogauss. The lines as obtained on the recorder are derivatives of the actual absorption lines.

In order to obtain an estimate of the number of spins contributing to the observed acoustic absorption lines, the latter are compared with the NMR lines for the same angle. The acoustic double-frequency absorption line is shown in Figs. 11(a) and 11(b) for θ equal to 90° and 60°; the acoustic single-frequency absorption line

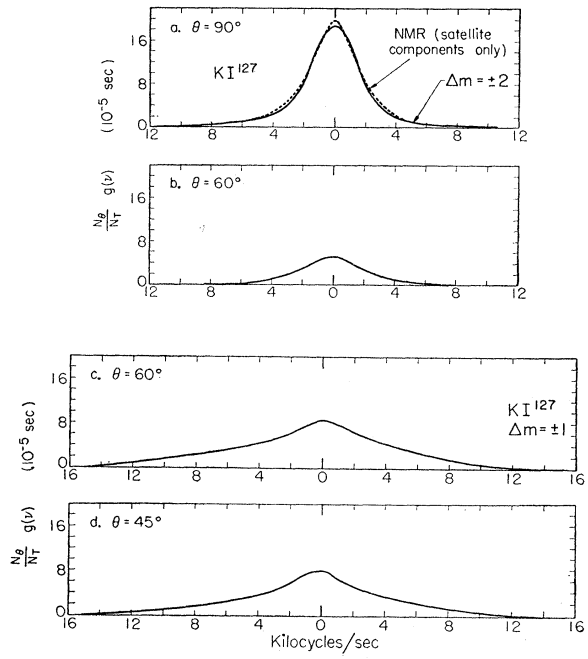

FIG. 11. NMR acoustic absorption lines for I^{127} in KI No. 1 at several angles θ between the acoustic axis and the external magnetic field. The double-frequency acoustic lines for $\theta=90°$ and 60° are shown in (a) and (b). The single-frequency lines for $\theta=60°$ and 45° are shown in (c) and (d). For comparison the 90° NMR line due to satellite transitions only is shown dotted in (a). This curve is taken from Fig. 6(a).

TABLE IV. Matching network characteristics.

	f (Mc/sec)	L_p (μh)	L_s (μh)	k	R_d (ohm)
KI No. 1	7.91	2.33	0.81	0.046	1000
KBr No. 1	9.75	1.50	2.0	0.064	2500

is shown in Figs. 11(c) and 11(d) for θ equal to 60° and 45°. A comparison between the acoustic double-frequency line and the corresponding NMR line due to satellite transitions only is made in Fig. 11(a). The superposition of the two lines is reasonable since the weighting of the inner to outer satellite transitions is nearly the same in the two cases. The differences between the two lines may be attributed to the larger modulation used to obtain the acoustic line, and to the increased broadening of the outer satellite component expected for the acoustic line (see Table I). This comparison enables us to conclude that approximately the same percentage of possible spins ($N/N_t=74\%$) contribute to the acoustic double-frequency line at 90° as contribute to the satellite part of the NMR line at 90°.

The angular variation of the peak absorption of the acoustic single- and double-frequency lines is shown in Fig. 12. The departure from the angular dependence predicted by the transition probabilities may be explained by the angular dependence of the line width. The result of dividing the $\Delta m=\pm 2$ curve of Fig. 12 by its transition probability gives a curve, shown in Fig. 7, which agrees closely with the angular variation of the peak intensity of the satellite part of the NMR line.

The double-frequency acoustic absorption line of Br^{81} in KBr No. 1 is shown in Fig. 13. The signal-to-noise of the bromine acoustic resonances in KBr was appreciably less than that of the iodine resonance in KI. The dashed line in Fig. 13(b) represents the satellite part of the NMR line as obtained from Fig. 8. As in the case of KI, a comparison of the acoustic and NMR data leads to the conclusion that the percentage of possible spins contributing to the Br^{81} acoustic double-frequency line at $\theta=90°$ is approximately the same as that (77%) contributing to the satellite part of the NMR line.

Quadrupole Coupling Coefficient

The additional attenuation of the acoustic wave due to nuclear absorption results, as described above, in a change in the acoustic impedance presented to the transducer. By means of the impedance matching and inverting network this change is reflected at the Pound oscillator as a change in the primary conductance, G_p.

TABLE V. Atomic characteristics.

	a (A)	N (10^{22}/cc)	Q (10^{-24} cm²)
KI^{127}	3.52	1.14	0.78
KBr^{81}	3.30	0.69	0.28

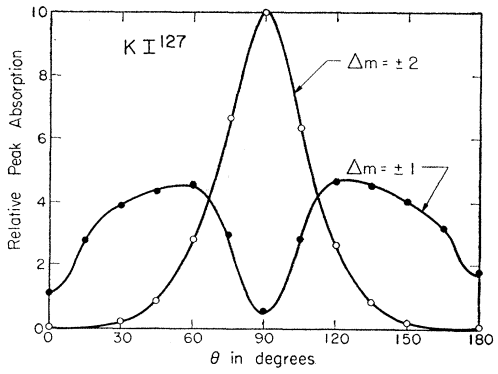

FIG. 12. Variation with θ of the relative peak intensity of the single- and double-frequency NMR acoustic absorption lines of I^{127} in KI No. 1. The result of dividing the double-frequency curve by the transition probability is shown in Fig. 7, where the resultant angular variation is seen to agree well with that observed for the satellite part of the NMR line.

Using Eq. (7) and circuit theory applied to the matching network, Fig. 4, we obtain an expression for the change in conductance:

$$\Delta G_p=\frac{k^2}{\omega^2 L_p L_s}\left(\frac{R_d}{R+R_d}\right)^2\frac{\rho c}{(2a)^2}Sl\alpha_n, \tag{8}$$

where k is the coefficient of coupling between the primary and secondary of the matching network.

The values of the quantities entering into Eq. (8) are given in Tables III and IV. Crystal characteristics are shown in Table V. The measured value of ΔG_p for I^{127} in KI for the double-frequency line at $\theta=90°$ was

$$\Delta G_p=10\times 10^{-10}\text{ mho}.$$

Substituting the above values into Eq. (8), we obtain for the NMR acoustic power absorption coefficient for

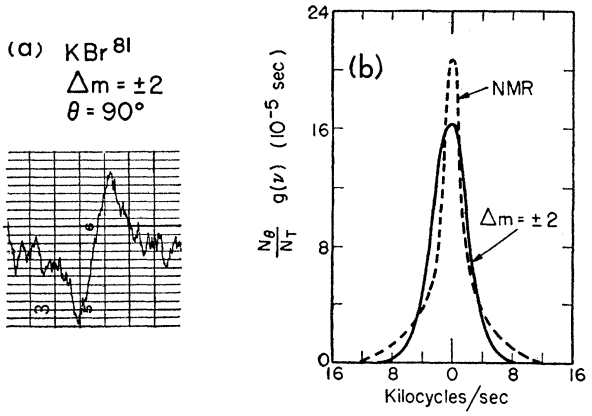

FIG. 13. (a) Recorder trace of the NMR acoustic double-frequency line of Br^{81} in KBr No. 1. $H_0=4.24$ kgauss, $f=9.75$ Mc/sec. af modulation was 2 gauss peak to peak. The signal to noise of the bromine acoustic resonance is seen to be considerably less than that of the iodine acoustic resonance in KI No. 1. (b) Integration of line shown at (a). For comparison the NMR absorption line due to the satellite transitions only is shown dashed. This curve is taken from Fig. 8(a).

TABLE VI. Quadrupole coupling constants (in Mc/sec).

	KI^{127}	KBr^{79}	Reference
e^2q_0Q (molecule)[a]	60	10	[b]
e^2q_1Q NMRAA	300	100	
e^2q_2Q (T_1)	26 000	4200	[c]

[a] Interatomic distances for molecule are 3.05 A for KI and 2.82 A for KBr. See reference 1.
[b] Honig, Mandel, Stitch, and Townes, Phys. Rev. **96**, 629 (1954).
[c] See reference 17.

I^{127} in KI,

$$2\alpha_n = 2.8\times10^{-8}\ \text{cm}^{-1}.$$

Similarly for KBr^{81}, by the same procedure, we obtain for the double-frequency 90° line,

$$\Delta G_p = 3.9\times10^{-11}\ \text{mho},$$
$$2\alpha_n = 1.2\times10^{-9}\ \text{cm}^{-1}.$$

Using Eqs. (6a) and (6c), and values of $2\alpha_n$ found above, we obtain:

$$(e^2q_1Q/h) = 300\ \text{Mc/sec for } I^{127} \text{ in KI},$$
$$(e^2q_1Q/h) = 82\ \text{Mc/sec for } Br^{81} \text{ in KBr}.$$

DISCUSSION

Considering the uncertainties in the various measurements and estimates which were made in arriving at the quadrupole coupling constant, it is the opinion of the authors that the value given is correct to within a factor of 1.4 for KI, and to within, perhaps, a somewhat larger factor for KBr. The largest uncertainty exists in the knowledge of the distribution of the acoustic energy in the sample—the effective area of the wave pattern. Other uncertainties occur in the measurement of line intensity and of transducer and network parameters, and in the estimate of N/N_t for the acoustic line. A pessimistic total of all of these gives a total uncertainty for the nuclear attenuation coefficient of a factor of two, which results in the factor of 1.4 for the quadrupole coupling.

The values of e^2q_1Q for KI^{127} and for KBr^{79} $[=(0.33/0.28)e^2q_1Q_{Br^{81}}]$ obtained by the NMR acoustic absorption technique are compared, in Table VI, with nuclear quadrupole coupling constants obtained from microwave spectroscopy and from measurements of spin-lattice relaxation times. The comparison is made with reference to the notation of (4), where the contributions of the static, first derivative and second derivative components of the field gradient are denoted, respectively by q_0, q_1, and q_2. Since the static coupling constant is zero for the crystal, e^2q_0Q for the molecule has been listed. e^2q_2Q has been obtained from the analysis by Van Kranendonk[18] of spin-lattice relaxation times. The values of relaxation times used are those given by Wikner and Hahn[19]: $T_1(KI^{127}) = 0.018$ sec, $T_1(KBr^{79}) = 0.074$ sec.

[18] J. Van Kranendonk, Physica **20**, 781 (1954).

TABLE VII. Amplification factors.

	KI^{127}	KBr^{79}
γ_0 (molecule)	42	10
γ_1 (NMRAA)	38	26
γ_2 (T_1)	850	260
γ (theoretical)	180	100

Attempts to explain nuclear quadrupole coupling constants in ionic crystals have been made using two approaches. The first, due to Van Kranendonk,[18] may be called the "ionic approach." He considers a one-parameter point charge model for the lattice, in which the ionic charge e is replaced by γe. γ is the "amplification factor" by which the quadrupole coupling exceeds that predicted on the basis of a simple ionic point charge model. The amplification is considered to be due to the polarization of the electron charge about the quadrupole nucleus by the nearest neighbor ions.[20,21] Calculations of γ for ionic crystals have been made by Das, Roy, Bersohn, and Wikner.[22–24] Bersohn[25] points out that although the ionic approach fails for the halide ions in alkali halide molecules (due perhaps to electron overlap) the theory may be more applicable to crystals, where the interatomic distances are larger than those in the diatomic molecule and where, therefore, electron overlap is less important.

The values of the amplification factor γ calculated on the basis of the ionic model are given in Table VII. Consistent with the notation above, we define γ_0, γ_1, and γ_2 as the values of the parameter γ required to fit, respectively, the observed quantities e^2q_0Q, e^2q_1Q, and e^2q_2Q. For the diatomic molecule, $e^2q_0Q = 2\gamma e^2Q/a^3$, where a is the interatomic distance. For the fcc crystal we assume a point charge model in which the quadrupole nucleus interacts only with the six nearest neighbor ions. On the application of a compressional sound wave along a cubic axis an axially symmetric field gradient with its symmetry axis in the direction of the sound propagation is created. We obtain:

$$e^2q_1Q = e^2a(dq/dr)Q = 12\gamma_1e^2Q/a^3,$$
$$e^2q_2Q = e^2a(d^2q/dr^2)Q = 48\gamma_2e^2Q/a^3.$$

In Table VII the values of γ calculated by Wikner and Das[23] for an ion in the field of an external point charge are also given. The values of γ_2 are calculated from

[19] E. G. Wikner and E. L. Hahn, Bull. Am. Phys. Soc. Ser. II, **3**, 325 (1958).
[20] R. M. Sternheimer, Phys. Rev. **105**, 158 (1957). References to earlier papers may be found in this reference.
[21] For a review of this subject see, e.g., the article by M. H. Cohen and F. Reif in *Solid State Physics*, edited by F. Seitz and D. Turnbull (Academic Press Inc., New York, 1957), Vol. V.
[22] T. P. Das and R. Bersohn, Phys. Rev. **102**, 733 (1956).
[23] Das, Roy, and Ghosh Roy, Phys. Rev. **104**, 1568 (1956).
[24] E. G. Wikner and T. P. Das, Phys. Rev. **109**, 360 (1958).
[25] R. Bersohn, J. Chem. Phys. **29**, 326 (1958).

Van Kranendonk's paper using the revised T_1's cited above.

The second theoretical approach, which may be termed the "covalent approach," has been treated in greatest detail by Yosida and Moriya.[26] They assume that the dominant contribution to the electric quadrupole coupling in cubic ionic crystals is due to the presence of a few percent covalent state, i.e., of an admixture of p-orbitals with the spherically symmetric ionic s-orbitals.[27] The modulation of the quadrupole interaction then is due to the dependence of the degree of covalency on the interatomic spacing. Yosida and Moriya estimate that the contribution from this effect to the thermal relaxation process is some 10^4 times greater than that computed on the basis of the single charge ionic model.

A comparison of the quadrupole coupling constants obtained in this experiment with results of other experimenters cannot be very direct, since no similar work for either KI or KBr has been reported. Otsuka,[28] using estimates of the density of dislocations introduced by plastic deformation of a KI crystal, arrived at a value of over 50 for the amplification factor, γ, for I^{127}. (Since most previous experimenters have interpreted their results in terms of the point charge model amplification factor γ, we will use this quantity for the comparison of results.) Jennings, Tantilla, and Kraus[6] performed an acoustic saturation experiment on NaI, from which they found a ratio γ_I/γ_{Na} for NaI of 10. If we use this ratio together with the value for γ_I obtained in this experiment (for KI) we obtain a value of about 4 for γ_{Na}. This may then be compared with values obtained for Na by other experimenters. Proctor and Robinson[5] in an acoustic saturation experiment on NaCl found γ_{Na} to be 1.4. Kawamura, Otsuka, and Ishiwatari,[29] from analysis of line shapes for a mixed alkali halide obtained a value of 10 for γ_{Na} in NaCl. The calculated value of γ for the Na ion is 5.6.[24]

[26] K. Yosida and T. Moriya, J. Phys. Soc. Japan **11**, 33 (1956).
[27] C. H. Townes and B. P. Dailey, J. Chem. Phys. **20**, 35 (1951).
[28] E. Otsuka, J. Phys. Soc. Japan **13**, 1155 (1958).

ACKNOWLEDGMENT

We wish to thank Mr. P. R. Malmberg for his assistance with many of the instrumental problems.

APPENDIX. DESIGN AND ADJUSTMENT OF MATCHING NETWORK

The exact circuit values of the matching network are not critical. The following rough recipe was found useful at frequencies near 8 Mc/sec: (1) measure resonant transducer resistance R on Q meter, (2) let $R_d=2R$, (3) choose L_2 so loaded Q of secondary is 10; $2\pi fL_2=(1/10)(2/3)R_t$, (4) let coefficient of coupling $k=0.04$, (5) let $2\pi fL_1=100$ ohms. This will cause an impedance of about 4000 ohms to be presented to the Pound-Watkins oscillator.

The adjustment of the matching network is more critical. Its purpose is to tune both primary and secondary to the sample resonance frequency. This is done while observing the primary resonance with a Q meter. A pattern as shown in Fig. 4 (bottom left) is seen. Correct tuning is indicated by equality of the side peaks and centering of the transducer peak between the side peaks. When the assembly is connected to the oscillator the latter's tuning condenser is set at the value used on the Q meter. When this condenser is tuned, a distinct locking-in of the oscillator frequency by the mechanical resonance is noticed. The correct setting gives a maximum impedance of the transducer peak. This can be observed as a minimum in the plate current of the oscillator tube.

[29] Kawamura, Otsuka, and Ishiwatari, J. Phys. Soc. Japan **11**, 1064 (1956).

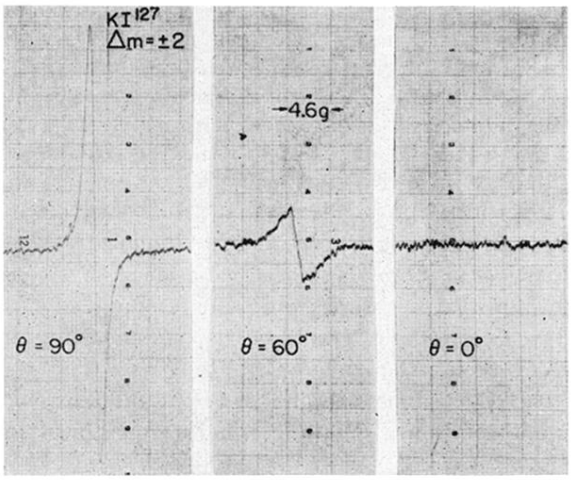

FIG. 10. Recorder traces of NMR acoustic absorption double-frequency lines of I^{127} in KI No. 1. The traces are derivatives of the actual absorption lines. θ is the angle between the acoustic axis and the direction of the external field. $H_0=4.6$ kgauss, $f=7.90$ Mc/sec. af modulation was 2 gauss peak to peak.

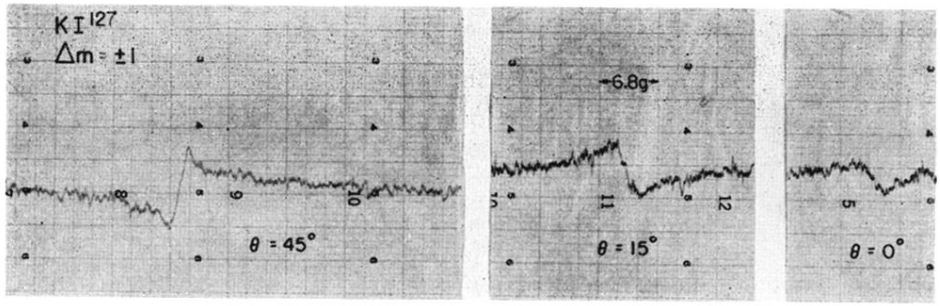

FIG. 9. Recorder traces of NMR acoustic absorption single-frequency lines of I^{127} in KI No. 1. The traces are derivatives of the actual absorption lines. θ is the angle between the acoustic axis and the direction of the external field. $H_0=9.22$ kgauss. $f=7.90$ Mc/sec. af modulation was 2 gauss peak to peak.